J Mater Sci (2011) 46:5959–5968
DOI 10.1007/s10853-011-5551-3

# Synthesis and applications of fluorescent-magnetic-bifunctional dansylated $Fe_3O_4$@$SiO_2$ nanoparticles

**Gang Liu · Huixia Wu · Haoran Zheng · Lihui Tang · He Hu · Hong Yang · Shiping Yang**

Received: 12 December 2010 / Accepted: 7 April 2011 / Published online: 20 April 2011


**Abstract** Bifunctional magnetic-luminescent dansylated $Fe_3O_4$@$SiO_2$ ($Fe_3O_4$@$SiO_2$-DNS) nanoparticles were fabricated by the nucleophilic substitution of dansyl chloride with primary amines of aminosilane-modified $Fe_3O_4$@$SiO_2$ core–shell nanostructures. The morphology and properties of the resultant $Fe_3O_4$@$SiO_2$-DNS nanoparticles were investigated by transmission electron microscopy, FT–IR spectra, UV–vis spectra, photoluminescence spectra, and vibrating sample magnetometry. The $Fe_3O_4$@$SiO_2$-DNS nanocomposites exhibit superparamagnetic behavior at room temperature, and can emit strong green light under the excitation of UV light. They show very low cytotoxicity against HeLa cells and negligible hemolysis activity. The $T_2$ relaxivity of $Fe_3O_4$@$SiO_2$-DNS in water was determined to be 114.6 Fe $mM^{-1}$ $s^{-1}$. Magnetic resonance (MR) imaging analysis coupled with confocal microscopy shows that $Fe_3O_4$@$SiO_2$-DNS can be uptaken by the cancer cells effectively. All these positive attributes make $Fe_3O_4$@$SiO_2$-DNS a promising candidate for both MR and fluorescent imaging applications.

## Introduction

Magnetic nanoparticles (especially iron oxide) have received increasing attention because of their unique physical and chemical properties and potential applications in various biomedical fields, such as targeted drug delivery, magnetic hyperthermia, magnetic resonance (MR) imaging, biosensing, and magnetic separation of biological materials [1–4]. Most of these applications require the nanoparticles to be chemically stable, biocompatible, and well-dispersed in a liquid medium. However, pristine nanoparticles of iron oxides tend to aggregate into large clusters because of anisotropic dipolar attraction, and thus their magnetic properties will be altered. Moreover, they can undergo rapid biodegradation when they are exposed to biological environment directly [5–8]. An efficacious solution is to encapsulate the nanoparticles in an inert shell, which inherently modifies their surface properties and prevents direct contact between the nanoparticles [7, 8].

Silica has been considered as an outstanding material for encapsulating the magnetic nanoparticles due to its good biocompatibility, excellent physicochemical stability, and facile multifunctionalization [9, 10]. There are two general ways to cover the magnetic nanoparticles with silica. One is the Stober method [11–13], the other is the reverse microemulsion method [6, 14–16]. Coating the nanoparticles with an inert silica shell yields a protective, inert, biocompatible, and hydrophilic surface with excellent anchoring points for surface conjugation with fluorescent molecules, poly(ethylene glycol) (PEG), and various biomolecules [17–21]. Importantly, the inert silica shell can also act as an excellent spacer for protecting the fluorescent molecules conjugated on the surface of silica from photoluminescence quenching induced by the magnetic cores [22].

5-Dimethylaminonaphthalene sulfonylchloride (dansyl chloride) is an important fluorescence derivatization reagent, which can react with amino, phenolic, and active hydroxyl groups under suitable experimental conditions

G. Liu · H. Wu (✉) · H. Zheng · L. Tang · H. Hu · H. Yang · S. Yang (✉)
The Key Laboratory of Resource Chemistry of Ministry of Education, College of Life and Environmental Science, Shanghai Normal University, 100 Guilin Road, Shanghai 200234, People's Republic of China
e-mail: wuhuixia@shnu.edu.cn

S. Yang
e-mail: shipingy@shnu.edu.cn

[23, 24]. It has been widely used as a fluorescence labeling reagent for fluorescence detection of amino acid and polypeptide, drugs, and other biomolecules with weak or no native fluorescence [23–26]. In this contribution, $Fe_3O_4$ nanoparticles (MNs) stabilized by the citric acid modification were prepared and subsequently coated with a silica layer by the reverse microemulsion method. The obtained $Fe_3O_4$@$SiO_2$ nanoparticles were then aminated through silanization for further covalently conjugating dansyl chloride to construct a multifunctional platform for both MR and fluorescent imaging applications (Scheme 1). The cytotoxicity and hemolysis activity of the resultant $Fe_3O_4$@$SiO_2$-DNS nanocomposites were evaluated. The cell uptake of $Fe_3O_4$@$SiO_2$-DNS was investigated by MR imaging and confocal luminescence imaging to explore the potential applications of the nanocomposites for bioimaging.

## Experimental section

### Reagents and instruments

$FeCl_2 \cdot 4H_2O$ was purchased from Acros Organics. Triton X-100 (>99%) and 3-aminopropyltriethoxysilane (APS) were obtained from Sigma-Aldrich. Dansyl chloride was provided by Alfa Aesar. Other chemicals and reagents were purchased from Sinopharm Chemical Reagent Co., Ltd. All reagents were used as received without further purification unless noted otherwise. Deionized water with resistivity higher than 18 MΩ cm was used in all experiments.

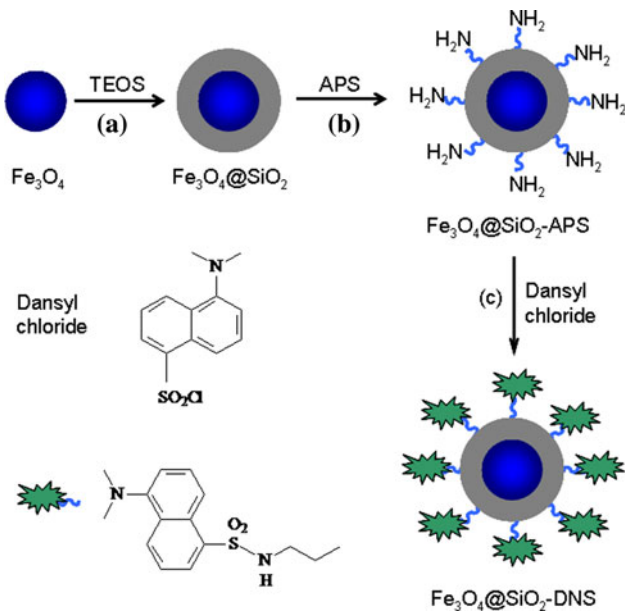


**Scheme 1** Schematic illustration for the synthesis of $Fe_3O_4$@$SiO_2$-DNS nanocomposites: **a** Coating the $Fe_3O_4$ nanoparticle with a silica layer by the reverse microemulsion method, **b** functionalizing $Fe_3O_4$@$SiO_2$ with 3-aminopropyltriethoxysilane (APS) and further conjugation with dansyl chloride (**c**) on the surface of the silica shell

Transmission electron microscope (TEM) images were performed with a JEOL JEM-2100 high-resolution transmission electron microscope (HR-TEM). X-ray diffraction (XRD) patterns were determined by a Rigaku DMAX 2000 diffractometer equipped with Cu/Kα radiation ($\lambda = 0.15405$ nm) (40 kV, 40 mA). The Fourier transform infrared (FT–IR) spectra were recorded on a Nicolet Avatar 370 FT–IR spectrophotometer using KBr pellets. The UV–vis absorption spectra were obtained with a UV-7502PC spectrophotometer. Thermal gravimetric analyses (TGA) were carried out by using a Shimadzu DTG-60H thermal analyzer in flowing air atmosphere (50 mL $min^{-1}$) at a heating rate of 10 °C $min^{-1}$. The photoluminescence (PL) spectra were taken on a Cary-Eclipse 500 spectrofluorometer (VARIAN) with a 60 W Xenon lamp as the excitation source. Hysteresis loop was measured with a vibrating sample magnetometer (VSM, Lakeshore 7407). Inductively coupled plasma-atomic emission spectroscopy (ICP-AES) determinations were carried out using a Vista-MPX ICP instrument (Varian).

### Synthesis of $Fe_3O_4$ nanoparticles

$Fe_3O_4$ nanoparticles were synthesized by the coprecipitation of ferrous and ferric salt (1:2 molar ratio) upon addition of aqueous ammonia under a nitrogen atmosphere. In brief, $FeCl_3 \cdot 6H_2O$ (10 mmol) and $FeCl_2 \cdot 4H_2O$ (5 mmol) were dissolved in 60 mL of water and heated to 80 °C. The pH of the mixed solution was adjusted to the range of 8.0–9.0 with aqueous ammonia under vigorous stirring, and the heating continued for 30 min. After introduction of citric acid aqueous solution (2 mL, 0.5 mg $mL^{-1}$), the reaction temperature was increased to 90 °C, and the mixture was stirred continuously for an additional 1.5 h. The solid was centrifuged, rinsed three times with deionized water, and then dispersed in water.

### Preparation of $Fe_3O_4$@$SiO_2$ core–shell nanoparticles

Typically, $Fe_3O_4$ (12 mg) dispersed in 2 mL of $H_2O$ was introduced into a microemulsion system composed of cyclohexane, Triton X-100 and hexanol (160 mL, 4:1:1, v/v/v). After 10 min of vigorous stirring, 0.7 mL of aqueous ammonia (28–30 wt%) was introduced into the mixture. Then tetraethoxy orthosilicate (TEOS, 1.35 mL) was added dropwise into the system under continuous mechanical agitation, and the optically transparent brown microemulsion mixture was stirred for another 16 h at room temperature. After that, ethanol was added to destabilize the microemulsion system. The resultant $Fe_3O_4$@$SiO_2$ nanoparticles were isolated via

centrifugation, washed three times in sequence with ethanol and distilled water, and then dried under vacuum at room temperature.

### Preparation of $Fe_3O_4$@$SiO_2$-DNS nanoparticles

$Fe_3O_4$@$SiO_2$ nanoparticles (25 mg) were dispersed in the mixed solvent of $H_2O$ and ethanol (200 mL, 1:4, v/v), then APS (2 mL) was added dropwise, and the mixture was allowed to react at 80 °C for 20 h under continuous stirring. The aminosilane-modified nanoparticles ($Fe_3O_4$@$SiO_2$-APS) were collected by a permanent magnet, washed with ethanol and distilled water three times, and then dried under vacuum. Afterwards, $Fe_3O_4$@$SiO_2$-APS (15 mg) was dispersed in 50 mL of dry acetone, then dansyl chloride (45 mg) and triethylamine (0.5 mL) were introduced, and the mixture was stirred at room temperature in dark for 24 h. The final product $Fe_3O_4$@$SiO_2$-DNS nanoparticles were separated by centrifugation, washed in sequence with acetone and ethanol, and then dried under vacuum.

### Cell culture

HeLa cell line was provided by the Institute of Biochemistry and Cell Biology, SIBS, CAS (China). Cells were cultured in regular growth medium consisting of DMEM (Dulbecco's Modified Eagle Medium) supplemented with 10% FBS (fetal bovine serum) in a humidified atmosphere with 5% $CO_2$ at 37 °C. They were routinely harvested by treatment with a trypsin–EDTA solution (0.25%).

### In vitro cytotoxicity of $Fe_3O_4$@$SiO_2$-DNS nanoparticles

In vitro cytotoxicity was evaluated by performing 3-(4,5-dimethylthiazol-2-yl)-2,5-diphenyltetrazolium bromide (MTT) assays on the HeLa cell line. Cells seeded in a 96-well cell culture plate at a density of $1 \times 10^4$ cells per well were cultured in 5% $CO_2$ at 37 °C for 24 h. Then the medium was replaced with a fresh medium containing different concentrations of $Fe_3O_4$@$SiO_2$-DNS nanoparticles (0, 10, 40, 80, and 120 mg $mL^{-1}$), and further incubated for 8 or 24 h. Finally, the cell viability was assessed by the MTT assay. The cytotoxicity was expressed as the percentage of cell viability compared to that of untreated control cells.

### Hemolysis assay

Human blood stabilized with EDTA was kindly provided by Shanghai Blood Center. The human red blood cells (HRBCs) were obtained by removing the serum from the blood by centrifugation. Following five times of washing with sterile isotonic PBS solution, the cells were diluted to 1/10 of their volume with PBS solution. Then 0.3 mL of the diluted HRBC suspension was mixed with: (a) 1.2 mL of deionized water as a positive control; (b) 1.2 mL of PBS as a negative control; (c) 1.2 mL of $Fe_3O_4$@$SiO_2$-DNS suspensions at concentrations of 50, 100, 200, and 400 μg $mL^{-1}$. The mixtures were shaken up gently, and then left to stand for 2 h at room temperature. Afterwards, the samples were centrifuged, and the absorbance of the supernatants was recorded from 500 to 650 nm using a Shimadzu UV-3101PC UV–vis absorption spectrophotometer. The hemolysis percentages of the samples were calculated by dividing the difference in absorbances between the sample and the negative control by the difference in absorbances at 541 nm between the positive and negative controls, and multiplying the resulting ratio by 100.

### In vitro MR imaging

MR imaging experiments were performed in a Niumag Imaging and Analyzing system NMI20-Analyst. The $T_1$- and $T_2$-weighted images were acquired using spin-echo imaging sequence with the following parameters: point resolution = 156 × 156 $\mu m^2$, section thickness = 0.6 mm, TE = 60 ms, TR = 4,000 ms, number of acquisitions = 1.

HeLa cells ($2 \times 10^6$) were incubated with 120 μg $mL^{-1}$ of $Fe_3O_4$@$SiO_2$-DNS for a given time at 37 °C in cell culture medium. The cells were then washed three times with PBS solution, collected, and suspended in 1.5 mL of PBS buffer containing 0.3% xanthan gum (1.5 mL Eppendorf tubes). The Eppendorf tubes were placed in a water bath and the $T_2$-weighted images were acquired with a 0.5 T MR scanner.

### Luminescence imaging

Confocal luminescence imaging was performed with an Olympus FV1000 laser scanning confocal microscope and a 60× oil-immersion objective lens. The HeLa cells seeded in a 35 mm glass bottom culture dish were washed with PBS buffer and then incubated with 50 μg $mL^{-1}$ of $Fe_3O_4$@$SiO_2$-DNS for 90 min at 37 °C. After washed 3 times with PBS, the cells were then stained with DAPI solution for 15 min.

## Results and discussion

### Synthesis and characterization of $Fe_3O_4$@$SiO_2$-DNS

The initial $Fe_3O_4$ nanoparticles (MNs) were prepared by the coprecipitation of ferrous and ferric salt and then stabilization by the citric acid modification [27]. Figure 1a shows the TEM image of the as-prepared MNs, which are

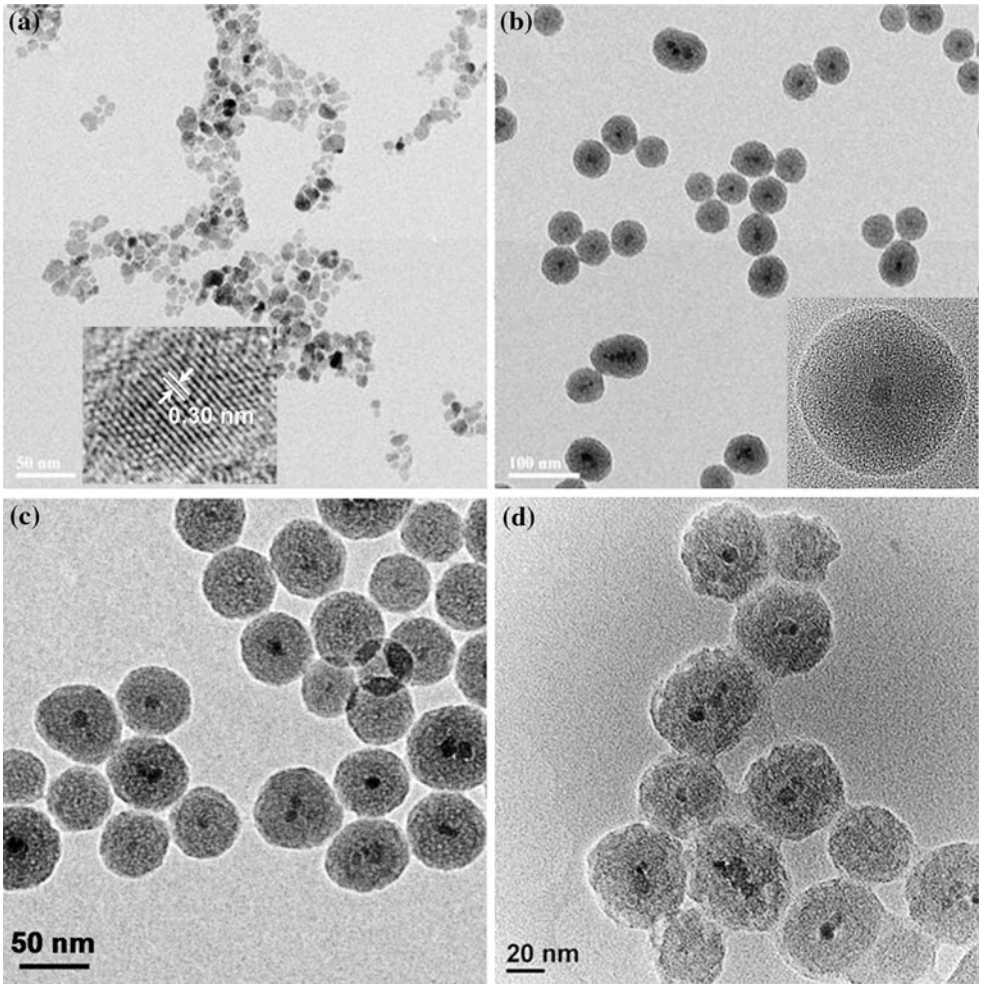


**Fig. 1** TEM images of MNs (**a**), $Fe_3O_4$@$SiO_2$ (**b**), $Fe_3O_4$@$SiO_2$-APS (**c**), and $Fe_3O_4$@$SiO_2$-DNS (**d**). *Inset* in **a** The HRTEM image of a $Fe_3O_4$ nanoparticle. *Inset* in **b** The higher magnification image of an individual $Fe_3O_4$@$SiO_2$ nanoparticle

nearly monodispersed with a mean particle diameter of 9.5 nm. The HRTEM image (the inset in Fig. 1a) of an individual nanoparticle reveals the lattice fringe with a lattice spacing of about 0.30 nm corresponding to the (2 2 0) plane of $Fe_3O_4$. Figure 2a presents the X-ray diffraction (XRD) pattern of MNs, which matches well with the standard cubic phase of $Fe_3O_4$ (JCPDS No. 65-3107) [28]. Figure 2c is the wide scan spectrum of the sample, in which the photoelectron lines at binding energy of about 286, 531, and 711 eV are attributed to C1 s, O1 s, and Fe 2p, respectively. In the inset of Fig. 2c, the peaks located at 710.6 and 724.0 eV correspond to Fe 2p3/2 and Fe 2p1/2, respectively. In contrast to $\gamma$-$Fe_2O_3$ XPS spectrum, it does not contain the charge transfer satellite of Fe 2p3/2 at 720 eV, which further confirms that the oxide in the sample was $Fe_3O_4$ [29]. In the FT–IR spectrum of MNs (not shown), two distinct peaks corresponding to asymmetric and symmetric C–O bonds can be observed at about 1623 and 1404 $cm^{-1}$, indicating the existence of citric acid on the surface of MNs [27]. Based on the weight loss of the sample at 100–300 °C, the content of CA was estimated to be about 6% [27].

The MNs were subsequently coated with a silica layer by the water-in-oil reverse microemulsion method to fabricate $Fe_3O_4$@$SiO_2$ core–shell nanoparticles. Figure 1b shows a representative TEM image of the resultant $Fe_3O_4$@$SiO_2$ nanoparticles. The monodisperse nanoparticles have nearly spherical nanostructures with a mean diameter of 46 nm, and the core–shell structure can be clearly observed due to the different electron contrast of $Fe_3O_4$ and $SiO_2$ [30]. The mean thickness of the silica shell layer is about 18 nm, which can be further tuned by changing the charging amount of TEOS [10]. The successful coating of silica shell on the surface of $Fe_3O_4$ was further demonstrated by the XRD pattern (Fig. 2b). In addition to the preserving reflections of iron oxide, a new broad diffraction peak appears at $2\theta = 23^{\circ}$ which can be attributed to the amorphous $SiO_2$ coating [31].

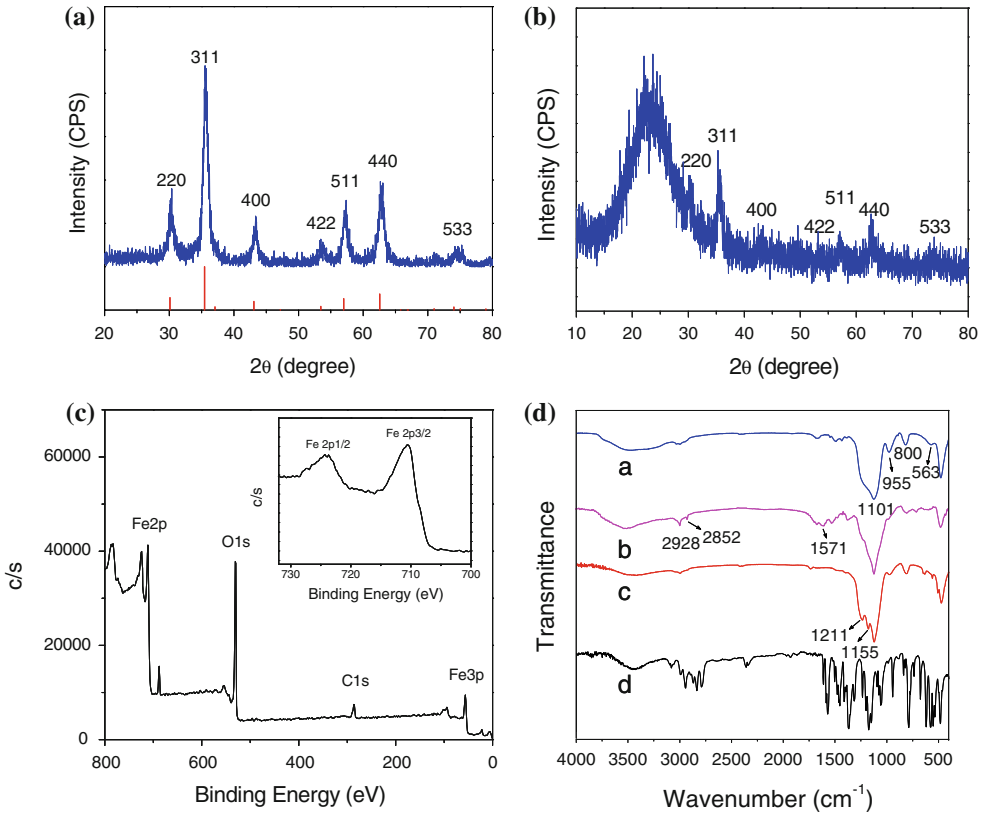


**Fig. 2** XRD patterns of MNs (**a**) and $Fe_3O_4$@$SiO_2$ (**b**); **c** XPS wide scan and Fe 2p peaks (the *inset*) of MNs; **d** FT–IR spectra of $Fe_3O_4$@$SiO_2$ (*a*), $Fe_3O_4$@$SiO_2$-APS (*b*), $Fe_3O_4$@$SiO_2$-DNS (*c*), and dansyl chloride (*d*)

The $SiO_2$ coating provides $Fe_3O_4$ nanoparticles with an active surface for further modification with functional molecules. To fabricate bifunctional nanostructure, $Fe_3O_4$@$SiO_2$ nanoparticles were subsequently modified with APS to immobilize amino groups onto the particle surfaces [32], followed by further conjugation of dansyl groups via nucleophilic substitution of dansyl chloride with the primary amines [33]. The unmodified $Fe_3O_4$@$SiO_2$ nanoparticles (Fig. 2d(a)) show the typical vibration bands of siliceous materials, such as that of asymmetric stretching of Si–O–Si at 1101 $cm^{-1}$, symmetric stretching of Si–O–Si at 800 $cm^{-1}$, and stretching vibrations of Si–OH groups at 955 $cm^{-1}$. The obvious absorbance at 563 $cm^{-1}$ is associated with the stretching and torsional vibration modes of the $Fe_3O_4$ [34, 35]. The successful functionalization of APS on $Fe_3O_4$@$SiO_2$ (Fig. 2d(b)) is confirmed by the presence of adsorption bands at 2928 and 2852 $cm^{-1}$, attributed to C–H asymmetric and symmetric stretching vibrations from propyl groups, and a characteristic band at 1571 $cm^{-1}$ due to inplane N–H bending of primary amines [36]. After

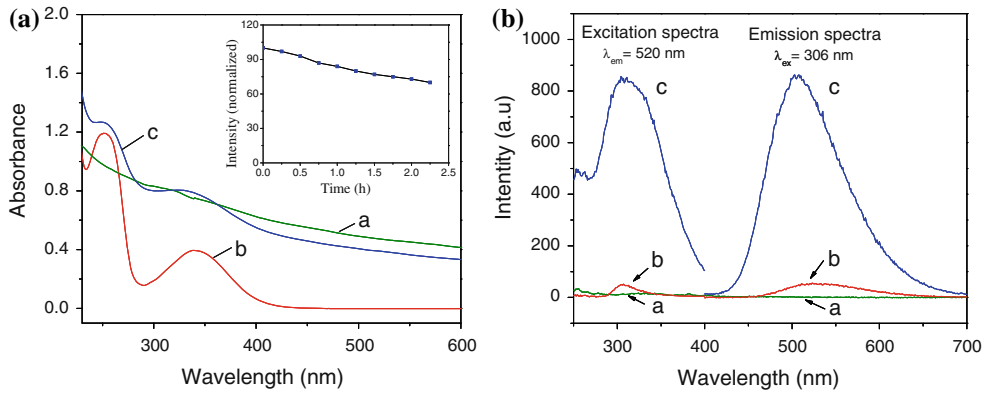


**Fig. 3** UV–vis spectra (**a**) and photoluminescence spectra (**b**) of $Fe_3O_4$@$SiO_2$-APS (*a*), dansyl chloride (*b*), and $Fe_3O_4$@$SiO_2$-DNS (*c*) dispersed in water. For UV–vis spectra: $Fe_3O_4$@$SiO_2$-APS, 0.5 mg $mL^{-1}$; dansyl chloride, 0.04 mg $mL^{-1}$; $Fe_3O_4$@$SiO_2$-DNS, 0.5 mg $mL^{-1}$. For photoluminescence spectra: the same concentration of 1 mg $mL^{-1}$ was used. The *inset* in **a** dependence of emission intensity on UV irradiation time ($\lambda_{ex}$ = 306 nm, the monitored $\lambda_{em}$ = 520 nm)

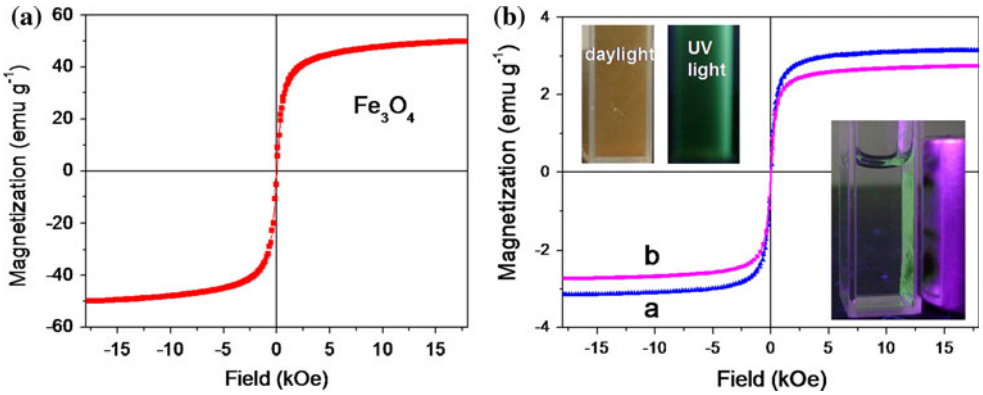


**Fig. 4** Room temperature magnetization curves of MNs (**a**), $Fe_3O_4$@$SiO_2$ (**b**(*a*)), and $Fe_3O_4$@$SiO_2$-DNS (**b**(*b*)). The *insets* in **b** The photographs of $Fe_3O_4$@$SiO_2$-DNS suspended in water taken under daylight lamp and 254 nm UV light (*upper-left*), and separated from solution by a magnet under UV light (*down-right*)

conjugation with dansyl groups (Fig. 2d(c)), the $SO_2$ stretching vibrations appear at 1211 $cm^{-1}$, and meanwhile, an additional band located at 1155 $cm^{-1}$ can be ascribed to the C–N stretching vibration of R-N$(CH_3)_2$ groups in the dansyl chromophore [37], demonstrating the successful conjugation of dansyl groups in $Fe_3O_4$@$SiO_2$-DNS. After surface functionalization, the formed $Fe_3O_4$@$SiO_2$-APS (Fig. 1c) and $Fe_3O_4$@$SiO_2$-DNS (Fig. 1d) still preserved the structure and morphology of $Fe_3O_4$@$SiO_2$.

The UV–vis spectra of dansyl chloride (0.04 mg $mL^{-1}$), $Fe_3O_4$@$SiO_2$-APS (0.5 mg $mL^{-1}$), and $Fe_3O_4$@$SiO_2$-DNS (0.5 mg $mL^{-1}$) are shown in Fig. 3a. $Fe_3O_4$@$SiO_2$-APS (Fig. 3a(a)) presents featureless absorption over the test wavelength range. Dansyl chloride (Fig. 3a(b)) exhibits intense absorption bands in the near UV spectral region ($\lambda_{max}$ = 253 and 340 nm) assigned to the $\pi$–$\pi^*$ and $n$–$\pi^*$ orbital transitions, respectively [38]. It can be seen from Fig. 3a(c) that these main bands of dansyl groups (251, 329 nm) still appear in the absorption spectrum of $Fe_3O_4$@$SiO_2$-DNS with somewhat blue shift due to the formation of fluorescent 5-dimethylamino-1-naphthalenesulphonamido (dansylamide) units. Figure 3b shows the excitation and emission spectra of $Fe_3O_4$@$SiO_2$-DNS, dansyl chloride, and $Fe_3O_4$@$SiO_2$-APS dispersed in water with the same concentration of 1 mg $mL^{-1}$. $Fe_3O_4$@$SiO_2$-APS does not show any emission at all, while dansyl chloride exhibits very weak fluorescence. For $Fe_3O_4$@$SiO_2$-DNS, a strong fluorescence band is observed in the visible region of 400–700 nm ($\lambda_{max}$ = 520 nm) under the optimal excitation wavelength ($\lambda_{ex}$ = 306 nm), which is assigned to the fluorescence emission of the dansylamide [38]. This indicates the sufficient silanization and subsequent efficient dansylamide formation of the dansylated sample, and meanwhile, the silica layer can effectively reduce the fluorescence quenching caused by the magnetic $Fe_3O_4$ cores. The dependence of emission intensity of $Fe_3O_4$@$SiO_2$-DNS on irradiation time was studied. As shown in the inset of Fig. 3a, the sample still displayed 73% of the original fluorescence intensity after 2 h of continuous exposure to UV light irradiation. The PL quantum yields of dansyl chloride and $Fe_3O_4$@$SiO_2$-DNS were determined by using quinoline sulfate ($\Phi_s$ = 0.55) as a fluorescence

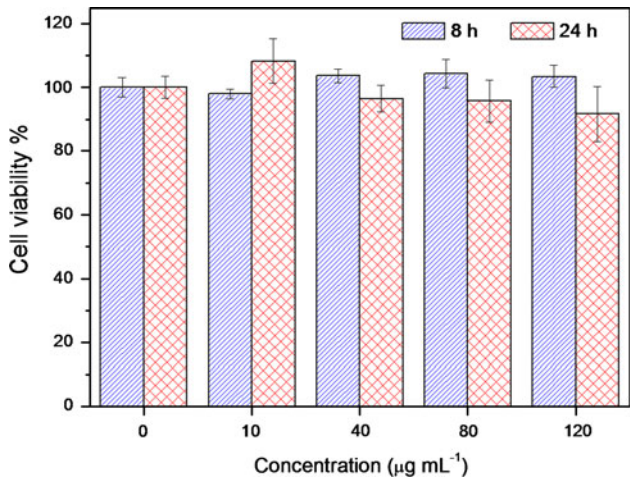


**Fig. 5** The effect of as-prepared $Fe_3O_4$@$SiO_2$-DNS on the viability of HeLa cells, as measured by MTT assays

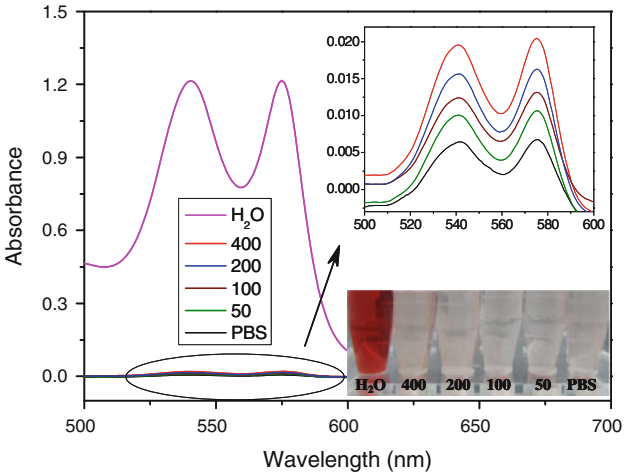


**Fig. 6** The UV–vis absorption spectra to detect the presence of hemoglobin in the supernatant of $Fe_3O_4$@$SiO_2$-DNS suspensions in PBS at concentrations of 50, 100, 200, and 400 μg $mL^{-1}$ using water and PBS solution as the positive and negative controls, respectively. The *down-right inset* the photograph of the supernatant of $Fe_3O_4$@$SiO_2$-DNS suspensions

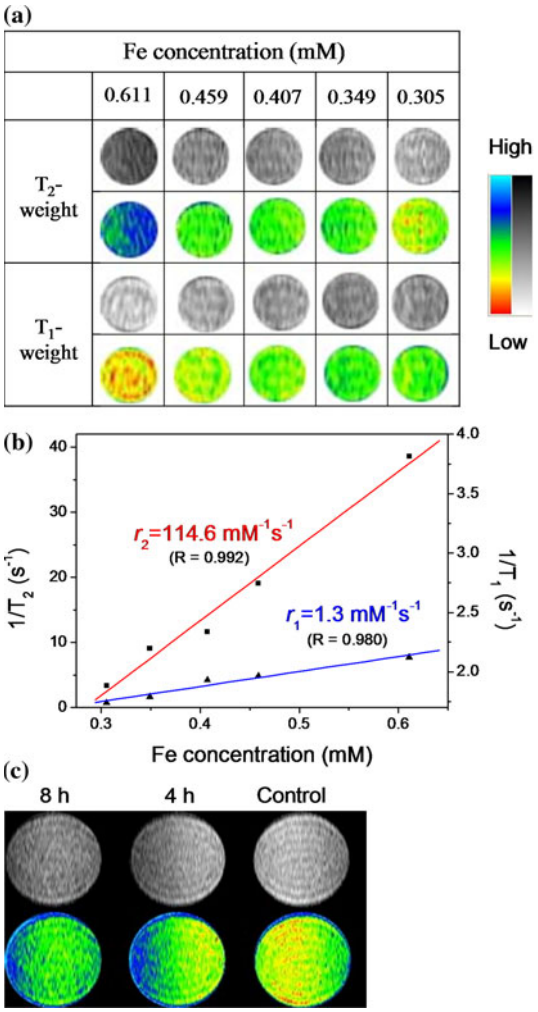


**Fig. 7** **a** $T_2$- and $T_1$-weighted MR images of $Fe_3O_4$@$SiO_2$-DNS suspended in water at different Fe concentrations; **b** Graphs of $R_2$ ($1/T_2$) and $R_1$ ($1/T_1$) relaxivities against the Fe concentration of $Fe_3O_4$@$SiO_2$-DNS; **c** MR imaging of HeLa cells after incubation with 120 μg $mL^{-1}$ of $Fe_3O_4$@$SiO_2$-DNS for 4 and 8 h. *Control* non-treated. The cells were suspended in 0.3% xanthan gum

standard [39]. $Fe_3O_4$@$SiO_2$-DNS ($\Phi = 0.26$) showed higher PL quantum yield than dansyl chloride ($\Phi = 0.06$).

The magnetic properties of the obtained materials were determined by VSM (Fig. 4). As shown in Fig. 4a, the MNs exhibit superparamagnetic behavior at 300 K with a saturation magnetization ($M_s$) of 50.0 emu $g^{-1}$. The superparamagnetic property at room temperature of as-prepared $Fe_3O_4$ is an important parameter for biomedical applications [40]. Compared with the MNs, the $M_s$ value of $Fe_3O_4$@$SiO_2$ decreased from 50.0 to 3.1 emu $g^{-1}$ due to the low density of the magnetic component in the core–shell nanostructure [41]. After conjugation of dansyl groups, the resultant $Fe_3O_4$@$SiO_2$-DNS shows an $M_s$ value of 2.7 emu $g^{-1}$, slightly lower than that of $Fe_3O_4$@$SiO_2$.

The hydrophilic character of the materials is a vital factor for biomedical applications. The as-prepared $Fe_3O_4$@$SiO_2$-DNS can be easily dispersed in PBS solution to form a well-dispersed suspension, and the nanocomposites emit the characteristic green light under the UV light (the upper-left inset in Fig. 4b). Moreover, the suspended nanocomposites with green light emission could be easily collected by the magnet (the down-right inset in Fig. 4b), suggesting that the dansyl groups have been firmly conjugated on the surface of $Fe_3O_4$@$SiO_2$ and the resultant nanocomposites can be manipulated by an external magnetic field.

## Cytotoxicity and HRBCs hemolytic behavior

The cytotoxicity of materials is crucial to their biomedical applications both in vitro and in vivo. To evaluate the cytotoxicity effect of $Fe_3O_4$@$SiO_2$-DNS, MTT assays were performed on the HeLa cell line. As shown in Fig. 5, the HeLa cells maintained greater than 80% cell viability even after 24 h of treatment with $Fe_3O_4$@$SiO_2$-DNS at a concentration as high as 120 μg $mL^{-1}$. These results clearly confirm the low cytotoxicity of $Fe_3O_4$@$SiO_2$-DNS nanoparticles within the experiment concentration range.

For in vivo bio-applications, the materials must have excellent blood compatibility, such as very low hemolysis effects when they are administrated by vein injection. Herein, to evaluate the blood compatibility of $Fe_3O_4$@$SiO_2$-DNS, a hemolysis assay was conducted according to the previous report [42]. During the hemolysis experiments, hemoglobin in the red blood cells will be released into the solution by hemolysis, and the resulting solution become visually red. The denser red color of corresponding solution means the higher hemolytic activity, therefore, the absorbance of the supernatant at 541 nm can be employed to estimate the quantity of hemoglobin released in the solution. The results of hemolysis assays in the supernatant are shown in Fig. 6. No visible hemolysis effect can be observed visually within the experiment concentration range of $Fe_3O_4$@$SiO_2$-DNS. The quantitative analysis by measuring the absorbance of the supernatant at 541 nm (hemoglobin) with UV–vis spectroscopy shows that no more than 1.09% hemolytic activity can be detected for $Fe_3O_4$@$SiO_2$-DNS even at a high concentration of 400 μg $mL^{-1}$. Consequently, it can be concluded that $Fe_3O_4$@$SiO_2$-DNS nanocomposites have neglectable hemolytic activity.

## In vitro MR imaging

The magnetic sensitivity of $Fe_3O_4$@$SiO_2$-DNS under magnetic field was investigated using MR imaging technique. $T_1$ and $T_2$ relaxation time of $Fe_3O_4$@$SiO_2$-DNS dispersed in water at different Fe concentration were measured at 0.5 T on a minispec MRI scanner. As shown in Fig. 7a, both $T_1$- and $T_2$-weighted images change

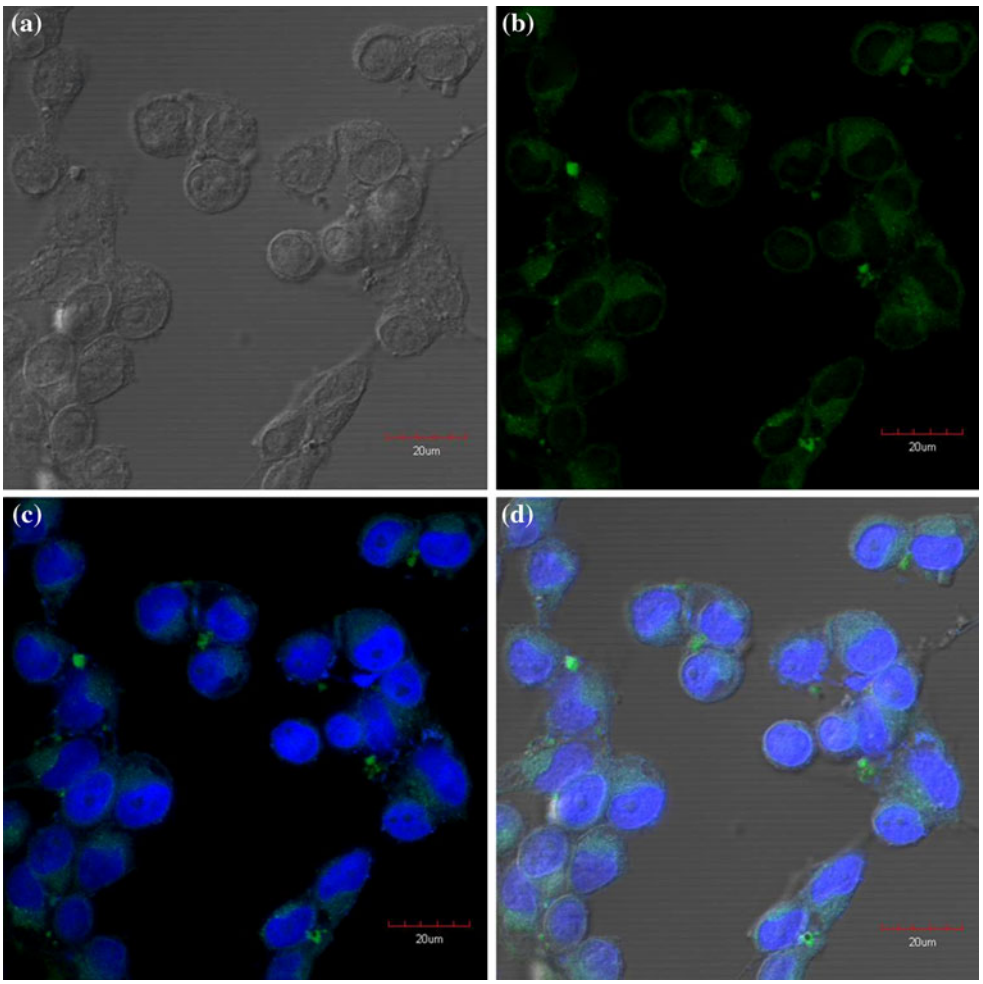


**Fig. 8** Fluorescent confocal micrographs of HeLa cells incubated with 50 μg $mL^{-1}$ of $Fe_3O_4$@$SiO_2$-DNS: **a** The brightfield image of the cells; **b** Fluorescent image excited at 488 nm to visualize the internalized $Fe_3O_4$@$SiO_2$-DNS by the cells; **c** Overlaid micrograph of image (**b**) with the fluorescent image of the cell nuclei stained with DAPI excited at 405 nm; **d** Overlaid micrograph of image (**c**) with (**a**)

remarkably in signal intensity with an increasing concentration of Fe nanoparticles. To further investigate the MRI contrast effect, the specific relaxivities ($r_1$ and $r_2$) were also measured. Figure 7b shows the longitudinal and transverse relaxation rates ($1/T_1$ and $1/T_2$) as a function of the Fe concentration (determined by ICP-AES) for $Fe_3O_4$@$SiO_2$-DNS. The $r_2$ and $r_1$ relaxivity coefficients were calculated to be 114.6 and 1.3 Fe $mM^{-1}$ $s^{-1}$, respectively. The high $r_2$ value and $r_2/r_1$ ratio of 88.2 indicate that the $Fe_3O_4$@$SiO_2$-DNS can be used as a favorable $T_2$ contrast agent.

In order to validate the diagnostic potential of the $Fe_3O_4$@$SiO_2$-DNS nanocomposites as a MR contrast agent, the $T_2$-weighted MR imaging of the HeLa cell line labeled with $Fe_3O_4$@$SiO_2$-DNS was investigated at a 0.5 T MRI scanner by suspending the cells in xanthan gum. As shown in Fig. 7c, the MR signal intensity in the cells after 4 and 8 h of incubation with 120 μg $mL^{-1}$ of $Fe_3O_4$@$SiO_2$-DNS exhibits an obvious MR contrast enhancement effect as compared with that of the background caused by the control cells. Furthermore, the MR image of 8 h exhibits stronger MR signal attenuation effect than that of 4 h, due to more nanoparticle uptake in the cells after 8 h of incubation [43]. The color maps of the $T_2$-weighted MR images are also shown in Fig. 7c, which reveals the similar results. Therefore, $Fe_3O_4$@$SiO_2$-DNS can serve as an effective $T_2$ imaging probe.

## Luminescence imaging

In order to explore the practical fluorescent bio-imaging application of $Fe_3O_4$@$SiO_2$-DNS nanoparticles, the sample was incubated in physiological conditions with HeLa cells for a given time, then the unbound nanoparticles were washed away, and the live cells were imaged using a

confocal microscope. As shown in Fig. 8, after incubation with 50 μg $mL^{-1}$ of $Fe_3O_4$@$SiO_2$-DNS nanoparticles in PBS (pH 7.4) for 90 min at 37 °C, strong green fluorescence from the nanoparticles is observed in the cytoplasm of the cells with high signal-to-background ratio, while untreated HeLa cells show negligible background fluorescence under similar imaging conditions, indicating that the nanoparticles have been internalized into the cells. The luminescence images confirm that $Fe_3O_4$@$SiO_2$-DNS nanoparticles can be effectively uptaken by the HeLa cells for cell imaging.

## Conclusions

In summary, bifunctional magnetic-luminescent dansylated $Fe_3O_4$@$SiO_2$ nanoparticles have been prepared by the nucleophilic substitution of dansyl chloride with primary amines of aminosilane-modified $Fe_3O_4$@$SiO_2$ core–shell nanostructures. The resultant $Fe_3O_4$@$SiO_2$-DNS nanocomposites display a strong green emission and a high $T_2$ relaxivity of 114.6 Fe $mM^{-1}$ $s^{-1}$ in aqueous solution. They show very low cytotoxicity, and can be uptaken by Hela cells effectively. The in vitro confocal microscopy and MR experiments demonstrate that $Fe_3O_4$@$SiO_2$-DNS can be used as a high-performance nanoprobe for cancer cell imaging. The hemolytic properties of the bifunctional nanoparticles were also investigated. The low hemolytic activity of the nanocomposites suggests the promising potential for in vivo applications of this material by the intravenous administration. The $Fe_3O_4$@$SiO_2$-DNS may be further conjugated with other biomolecules (e.g., antibody and peptides) to construct multifunctional systems for bioimaging of various biological systems. Moreover, the dansylated $Fe_3O_4$@$SiO_2$ can be used for various purposes of sensory testing, because the emission from dansyl and its derivatives show considerable variation in the Stokes shift as a function of its surroundings.

**Acknowledgements** This study is supported by the National Natural Science Foundation of China (Grant no. 50972092, 20971086), the Science and Technology Commission of Shanghai Municipality (065212050, S30406), Special Foundation of China Postdoctoral Science Foundation (201003282), the Shanghai Key Laboratory of the Rare Earth Functional Materials (07dz22303), the Shanghai Municipal Education Commission (10ZZ84), Leading Academic Discipline Project of Shanghai Normal University (DZL806), and the Key Subject of Education Ministry of China (210075).

## References

1. Tran N, Webster TJ (2010) J Mater Chem 20:8760
2. Sandhu A, Handa H, Abe M (2010) Nanotechnology 21:442001
3. Hao R, Xing RJ, Xu ZC, Hou YL, Gao S, Sun SH (2010) Adv Mater 22:2729
4. Veiseh O, Gunn JW, Zhang MQ (2010) Adv Drug Deliv Rev 62:284
5. Lu Y, Yin YD, Mayers BT, Xia YN (2002) Nano Lett 2:183
6. Yang HH, Zhang SQ, Chen XL, Zhuang ZX, Xu JG, Wang XR (2004) Anal Chem 76:1316
7. Barnakov YA, Yu MH, Rosenzweig Z (2005) Langmuir 21:7524
8. He R, You XG, Shao J, Gao F, Pan BF, Cui DX (2007) Nanotechnology 18:315601
9. Lai W, Garino J, Ducheyne P (2002) Biomaterials 23:213
10. Stjerndahl M, Andersson M, Hall HE, Pajerowski DM, Meisel MW, Duran RS (2008) Langmuir 24:3532
11. Stober W, Fink A, Bohn EW (1968) J Colloid Interface Sci 26:62
12. Ma DL, Veres T, Clim L, Normandin F, Guan JW, Kingston D, Simard B (2007) J Phys Chem C 111:1999
13. Wang L, Tan WH (2006) Nano Lett 6:84
14. Zhao XJ, Bagwe RP, Tan WH (2004) Adv Mater 16:173
15. Santra S, Zhang P, Wang KM, Tapec R, Tan WH (2001) Anal Chem 73:4988
16. Chen F, Bu WB, Chen Y, Fan YC, He QJ, Zhu M, Liu XH, Zhou LP, Zhang SJ, Peng WJ, Shi JL (2009) Chem Asian J 4:1809
17. Yoon TJ, Yu KN, Kim E, Kim JS, Kim BG, Yun SH, Sohn BH, Cho MH, Lee JK, Park SB (2006) Small 2:209
18. Yang H, Zhuang YM, Hu H, Du XX, Zhang CX, Shi XY, Wu HX, Yang SP (2010) Adv Funct Mater 20:1733
19. Zhang BB, Chen BD, Wang YL, Guo FF, Li ZQ, Shi DL (2011) J Colloid Interface Sci 353:426
20. Wang XX, Zhong JY, Liu Y, Wen AX, Shan Z, Yang WS (2010) Acta Chim Sinica 68:2063
21. Lu CW, Hung Y, Hsiao JK, Yao M, Chung TH, Lin YS, Wu SH, Hsu SC, Liu HM, Mou CY, Yang CS, Huang DM, Chen YC (2007) Nano Lett 7:149
22. Schartl W (2010) Nanoscale 2:829
23. Cruces-Blanco C, Carretero AS, Boyle EM, Gutierrez AF (1999) Talanta 50:1099
24. Tong AJ, Wu YG, Li LD (1996) Talanta 43:1429
25. Qi L, Yang GL (2009) Electrophoresis 30:2882
26. Sanchez FG, Blanco CC (1991) Analyst 116:851
27. Sahoo Y, Goodarzi A, Swihart MT, Ohulchanskyy TY, Kaur N, Furlani EP, Prasad PN (2005) J Phys Chem B 109:3879
28. Park J, An KJ, Hwang YS, Park JG, Noh HJ, Kim JY, Park JH, Hwang NM, Hyeon T (2004) Nat Mater 3:891
29. Morel AL, Nikitenko SI, Gionnet K, Alain Wattiaux, Lai-Kee-Him J, Labrugere C, Chevalier B, Deleris G, Petibois C, Brisson A, Simonoff M (2008) ACS Nano 2:847
30. Zhou JF, Meng LJ, Lu QH, Fu JW, Huang XB (2009) Chem Commun 42:6370
31. Jana NR, Earhart C, Ying JY (2007) Chem Mater 19:5074
32. Abboud M, Turner M, Duguet E, Fontanille M (1997) J Mater Chem 7:1527
33. Albala R, Olmos D, Aznar AJ, Baselga J, Gonzalez-Benito J (2004) J Colloid Interface Sci 277:71
34. Wang LY, Bao J, Wang L, Zhang F, Li YD (2006) Chem Eur J 12:6341
35. Guo SJ, Li D, Zhang LM, Li J, Wang EK (2009) Biomaterials 30:1881
36. Cao HN, He J, Deng L, Gao XQ (2009) Appl Surf Sci 255:7974
37. Griesser T, Hofler T, Temmel S, Kern W, Trimmel G (2007) Chem Mater 19:3011
38. Vogtle F, Gestermann S, Kauffmann C, Ceroni P, Vicinelli V, De Cola L, Balzani V (1999) J Am Chem Soc 121:12161
39. Li ZY, Xia JL, Liang JH, Yuan JJ, Jin GJ, Yin J, Yu GA, Liu SH (2011) Dyes Pigments 90:290

40. Wang Y, Ng YW, Chen Y, Shuter B, Yi J, Ding J, Wang SC, Feng SS (2008) Adv Funct Mater 18:308
41. Salgueirino-Maceira V, Correa-Duarte MA, Spasova M, Liz-Marzan LM, Farle M (2006) Adv Funct Mater 16:509
42. Slowing II, Wu CW, Vivero-Escoto JL, Lin VSY (2009) Small 5:57
43. Yang H, Zhang JJ, Tian QW, Hu H, Fang Y, Wu HX, Yang SP (2010) J Magn Magn Mater 322:973